JACC: CARDIOVASCULAR IMAGING VOL. 2, NO. 12, 2009

ISSN 1936-878X/09/$36.00
PUBLISHED BY ELSEVIER INC. DOI:10.1016/j.jcmg.2009.09.012

Feasibility of Noninvasive Assessment of Thin-Cap Fibroatheroma by Multidetector Computed Tomography

Manabu Kashiwagi, MD, Atsushi Tanaka, MD, Hironori Kitabata, MD, Hiroto Tsujioka, MD, Hideaki Kataiwa, MD, Kenichi Komukai, MD, Takashi Tanimoto, MD, Kazushi Takemoto, MT, Shigeho Takarada, MD, Takashi Kubo, MD, Kumiko Hirata, MD, Nobuo Nakamura, MD, Masato Mizukoshi, MD, Toshio Imanishi, MD, Takashi Akasaka, MD

Wakayama, Japan

OBJECTIVES The purpose of this study was to investigate whether multidetector computed tomography (MDCT) can noninvasively help assess thin-cap fibroatheroma (TCFA).

BACKGROUND Plaque rupture and thrombus formation play key roles in the onset of acute coronary syndrome. TCFA is recognized as a precursor lesion for plaque rupture, and MDCT angiography can potentially help identify plaques prone to rupture.

METHODS We enrolled 105 patients with coronary artery disease (acute coronary syndromes, n = 31; stable angina pectoris, n = 74). Culprit lesions were assessed by both MDCT and optical coherence tomography (OCT). Patients were divided into a TCFA and a non-TCFA group according to OCT findings; clinical and MDCT observations were compared for 2 groups.

RESULTS There were no differences in patients' characteristics between the 2 groups. OCT revealed 25 TCFAs at the culprit site in 105 patients. Acute coronary syndrome was more frequent in the TCFA group than in the non-TCFA group (52% vs. 23%, $p = 0.01$). High-sensitive C-reactive protein was higher in the TCFA group (0.32 ± 0.32 mg/dl vs. 0.17 ± 0.16 mg/dl, $p < 0.001$). Positive remodeling identified by MDCT was observed more frequently in the TCFA group than in the non-TCFA group (76% vs. 31%, $p < 0.001$). Computed tomography attenuation value of the culprit plaque in the TCFA group was lower than that in the non-TCFA group (35.1 ± 32.3 HU vs. 62.0 ± 33.6 HU, $p < 0.001$). The frequency of ring-like enhancement in the TCFA group was higher than in the non-TCFA group (44% vs. 4%, $p < 0.0001$). The sensitivity, specificity, positive predictive value, and negative predictive value of ring-like enhancement for detecting TCFA are 44%, 96%, 79%, and 85%, respectively. By stepwise regression, the ring-like enhancement, high-sensitive C-reactive protein, and diagnosis of acute events were associated with the presence of TCFA at the culprit site.

CONCLUSIONS MDCT can identify differences in plaque morphologies between TCFA and non-TCFA. From our results, MDCT may provide for the noninvasive assessment of vulnerable plaque. (J Am Coll Cardiol Img 2009;2:1412–9) © 2009 by the American College of Cardiology Foundation

From the Department of Cardiovascular Medicine, Wakayama Medical University, Wakayama, Japan.
Manuscript received June 22, 2009; revised manuscript received September 28, 2009, accepted September 29, 2009.

Acute coronary syndrome (ACS) results from rupture or ulcer formation of atheromatous plaque (1,2). Pathological studies have proposed that thin-cap fibroatheroma (TCFA) is 1 type of precursor lesion for rupture (3). Intravascular optical coherence tomography (OCT) offers a high-resolution imaging method for plaque characterization; its resolution is approximately 10 to 20 μm, which is about 10-fold higher than intravascular ultrasound (IVUS) (4–9). OCT can be used to determine the thickness of the fibrous cap (10). A recent OCT study reported that TCFA is more frequent in unstable lesions (9).

Recent advances in multidetector computed tomography (MDCT) technology have allowed for the noninvasive assessment of coronary artery stenosis and plaque characterization (11–14). Moreover, MDCT studies have revealed the differences in the plaque morphologies of culprit lesions in patients with ACS (15,16). A ring-like sign from MDCT observation possibly representing extensive necrotic core is related to plaque rupture and no-reflow phenomenon during percutaneous coronary intervention (PCI) (17,18). Therefore, we hypothesized that MDCT also could assess TCFA. To test our hypothesis, we investigated whether 64-slice MDCT could noninvasively assess a TCFA, as assessed by OCT, in patients with coronary artery disease.

METHODS

Population. We enrolled 105 consecutive patients who underwent both MDCT before coronary angiography and OCT in this study. The definition of ACS (non–ST-segment elevation myocardial infarction, unstable angina) established by a previous multicenter MDCT study was employed (19).

The culprit lesions were identified using a combination of electrocardiographic (ECG) findings, left ventricular wall motion abnormalities in echocardiography, and/or scintigraphy in correspondence with most stenotic site on coronary angiography.

Exclusion criteria were nonadequate MDCT imaging due to heavily calcified lesions by visual estimation, a culprit lesion in the left main coronary artery, renal insufficiency (serum creatinine >1.5 mg/dl), artificial dialysis, and cardiogenic shock. Written informed consent was obtained from all patients for participation in this study, and the study protocol was approved by our hospital ethics committee. The study was carried out according to the Declaration of Helsinki.

Scanning and imaging protocol of MDCT. MDCT was performed using 64-slice detector computed tomography (CT) (Lightspeed VCT, GE Healthcare UK Ltd., Little Chalfont, United Kingdom). All patients with a heart rate >70 beats/min received a beta-blocker (20 to 40 mg oral metoprolol or intravenous 1 to 2 mg propranolol) before the CT scan. A bolus of 65 ml of contrast (Omnipaque 350, Daiichi Pharmaceutical Co., Ltd., Tokyo, Japan) was injected intravenously at a flow rate of 3.5 to 4.5 ml/s followed by a 30 ml saline injection at the same flow rate.

Scans were obtained with a collimation of 0.625 mm per detector row, a table feed of 7.2 to 8.0 mm/rotation, a tube current of 500 to 800 mA depending on patient body weight, a tube voltage of 120 kV, and a gantry rotation speed of 350 ms. An estimated mean effective radiation dose was approximately 13 to 16 mSv. Trans-axial images were reconstructed using a medium sharp convolution kernel with an image matrix of 512 × 512 pixels, slice thickness of 0.625 mm, and an increment of 0.625 mm using an ECG-gated 1-segment scan algorithm with a resulting temporal resolution of 175 ms in the center of rotation. Images were initially reconstructed at 65% of the cardiac cycles. If we could not reconstruct the adequate image for analysis at 65% of the cardiac cycle, we reconstructed at 60% or 70% of the cardiac cycle.

Image analysis of coronary arteries by MDCT-. The analysis of 64-slice MDCT image data was performed by 2 experienced readers (H.T. and S.T.) blinded to OCT findings. We used the analysis system (Advantage Workstation VolumeShare and Cardiac Analysis PRO, GE Healthcare UK Ltd.) for CT analysis. Quantitative measurements were performed under concordance of 2 observers. The corresponding images of angiograms and MDCT were identified by the distances from 2 landmarks, such as side branches or ostium.

Maximum intensity projections were used to identify coronary lesions, and multiplanar reconstructions in 2 orthogonal longitudinal axes across the coronary lumen were utilized to classify lesions as significant stenosis, which was defined as a diameter reduction >50%.

Outer vessel area and arterial remodeling index (RI) were assessed by cross-sectional images. The arterial RI was defined as the ratio between the

ABBREVIATIONS AND ACRONYMS

ACS = acute coronary syndrome
CT = computed tomography
IVUS = intravascular ultrasound
MDCT = multidetector computed tomography
OCT = optical coherence tomography
PCI = percutaneous coronary intervention
TCFA = thin-cap fibroatheroma

JACC: CARDIOVASCULAR IMAGING, VOL. 2, NO. 12, 2009
DECEMBER 2009:1412–9

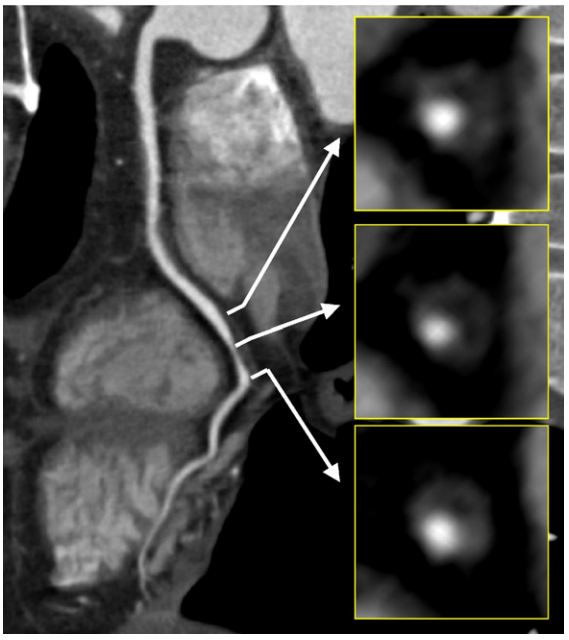

Figure 1. Ring-Like Enhancement Assessed by MDCT

The representative image of the ring-like enhancement assessed by multidetector computed tomography (MDCT) is shown. Contrast medium enhanced the outer area of the plaque to make it appear like a ring. This ring-like enhancement is located in the distal portion of right coronary artery.

outer vessel area at the site of maximal luminal narrowing and the mean of the proximal and distal reference sites. Positive remodeling was defined as an RI >1.05.

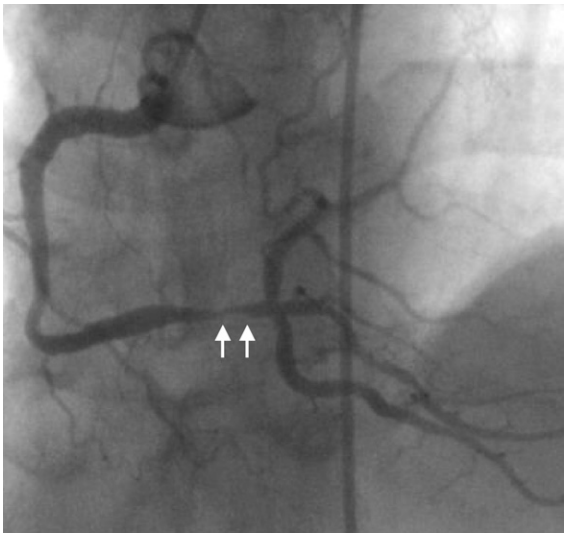

Figure 2. Invasive Coronary Angiography

Invasive coronary angiography revealed significant stenosis located in the distal portion of right coronary artery **(white arrows)** as well as multidetector computed tomography presented.

Calcium depositions were classified as long (>3 mm), short (≤3 mm), or none. The evaluation of coronary plaques were performed at a width representing 200% of the mean lumen intensity and at a level representing 65% of that. The CT attenuation values of plaques were measured in multiple (at least 3 sections) cross-sectional images along the plaque by 5-pixel regions of interest at multiple sites in the plaque and averaged. If the culprit plaque had any calcified components, regions of interest were positioned on the noncalcified area (17).

Ring-like enhancement. The definition of ring-like enhancement was used according to our previously published criterion: 1) the presence of a ring of high attenuation around certain coronary artery plaque; and 2) the CT attenuation of a ring presenting higher than those of the adjacent plaque and no >130 HU in order to differentiate from calcium depositions (18). A representative case of the ring-like enhancement assessed by MDCT and corresponding angiography and OCT images are presented in Figures 1 to 4.

Invasive coronary angiography. Cardiac catheterization was performed by a percutaneous femoral approach with a 5-F catheter. The culprit lesion was determined on the basis of the findings by a coronary angiogram as well as an ECG and transthoracic echocardiogram. Coronary angiograms were reviewed separately by independent observers (T.T. and N.N.). Quantitative angiography was performed offline using a CMS-QCA system (CMS-MEDIS, Medical Imaging Systems, Leiden, the Netherlands).

OCT imaging protocol. The culprit lesion was observed by OCT before PCI. A 0.016-inch OCT catheter (ImageWire, LightLab Imaging, Westford, Massachusetts) was advanced to the distal end of the culprit lesion through a microcatheter. All OCT image acquisitions were performed with the continuous flushing method (20). Serial OCT images were obtained using the automatic pullback function at a rate of 1.0 mm/s.

OCT image analysis. Three independent, experienced investigators (H.K., H.K., and M.M.) who were blinded to MDCT images, analyzed OCT images. The corresponding images of angiograms and OCT were identified by the distances from 2 landmarks, such as side branches or ostium. OCT images were analyzed using validated criteria for plaque characterization, and fibrous cap thickness was determined as reported previously (21,22). Lipids were semi-quantified as the number of involved quadrants on the cross-sectional OCT

image. When lipids were present in more than 2 quadrants in any of the images within a plaque, it was considered a lipid-rich plaque. For each patient, the cross-sectional image with the highest number of lipid quadrants was used for analysis. TCFA was defined as a plaque with lipid content in more than 2 quadrants and the thinnest part of the fibrous cap measuring <70 μm (4,9,21,23). Patients were divided into a TCFA group and a non-TCFA group according to OCT findings.

Statistical analysis. Statistical analysis was performed using SPSS software for Windows version 11.0 (SPSS Inc., Chicago, Illinois). Results are expressed as mean ± SD for approximately normally distributed variables and median (interquartile range) for skewed variables. Qualitative data are presented as numbers (%). Differences between the 2 groups were tested by the unpaired *t* test for approximately normally distributed variables, by Mann-Whitney *U* test for skewed variables, and by Fisher exact test for categorical variables. Receiver-operating characteristic curve analysis was used to determine the best cutoff value for RI and CT attenuation value for diagnosis of TCFA. Also, stepwise regression analysis was applied to determine which variables, including age, gender, high-sensitive C-reactive protein value, ACS, CT attenuation value, RI, and ring-like enhancement, were more closely associated with the presence of TCFA. These statistical analyses were made without correction for multiple comparisons. A p value <0.05 was considered statistically significant.

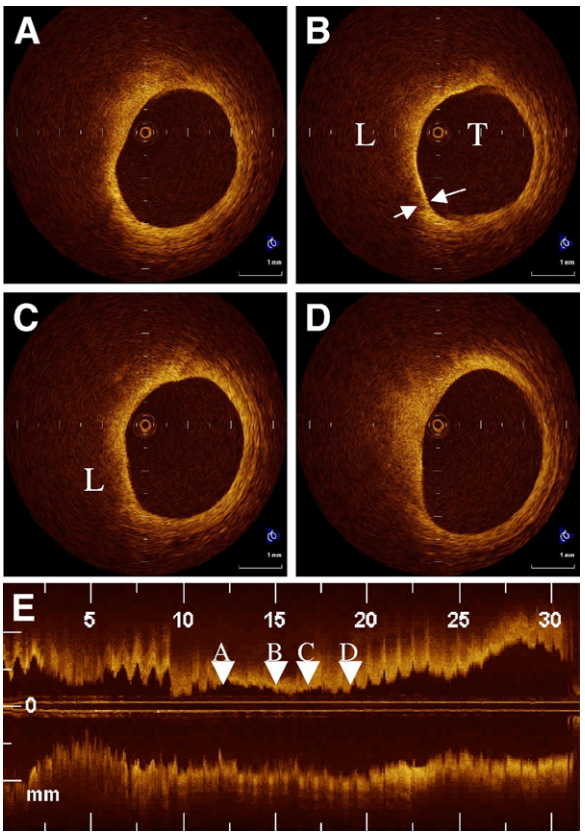

Figure 3. Corresponding OCT Images

Corresponding optical coherence tomography (OCT) images at the lesion with ring-like enhancement are shown. **A to D** are cross-sectional views of the coronary artery, and **E** is a longitudinal view. **B and C** show a lipid-rich plaque **(L)** and **B** especially shows a thin fibrous cap **(white arrows, T)**.

RESULTS

We excluded 20 patients for severe calcification, 6 patients for left main coronary artery, and 12 patients for renal insufficiency from the originally enrolled 143 patients. The baseline characteristics are demonstrated in Table 1. For all ACS patients, MDCT, as well as invasive angiography and PCI, were performed within 48 h after admission. No significant difference was found in the baseline characteristics, except for ACS and CRP level, between the 2 groups. Angiographic findings are summarized in Table 2. There were no differences in angiographic findings between the 2 groups.

The mean time between MDCT and OCT examination was 5 ± 4 days. MDCT findings for both groups are summarized in Table 3. The ring-like enhancement, RI, and positive remodeling were higher in the TCFA group than in the non-TCFA group. The sensitivity, specificity, positive predictive value, and negative predicative value of ring-like enhancement for detecting TCFA are 44%, 96%, 79%, and 85%, respectively. From the receiver operating curve, the best cutoff values of RI and CT attenuation to predict TCFA were 1.11 and 20 HU, respectively. The sensitivity and specificity of RI were 64% and 88%, and those of CT attenuation were 44% and 88%, respectively. Table 4 shows the results of stepwise regression analysis. The ring-like enhancement, high-sensitive C-reactive protein, and the diagnosis of ACS were associated with the presence of TCFA at the culprit site.

The ring-like enhancement was observed more frequently in ruptured plaque (ruptured plaque 43% vs. nonruptured plaque 15%, p = 0.03), but not in plaque with thrombus (plaque with thrombus 57% vs. plaque without thrombus 35%, p = 0.13). It may be possible that motion artifacts prevented the visualization of "ring-like" enhancement in some

JACC: CARDIOVASCULAR IMAGING, VOL. 2, NO. 12, 2009
DECEMBER 2009:1412–9

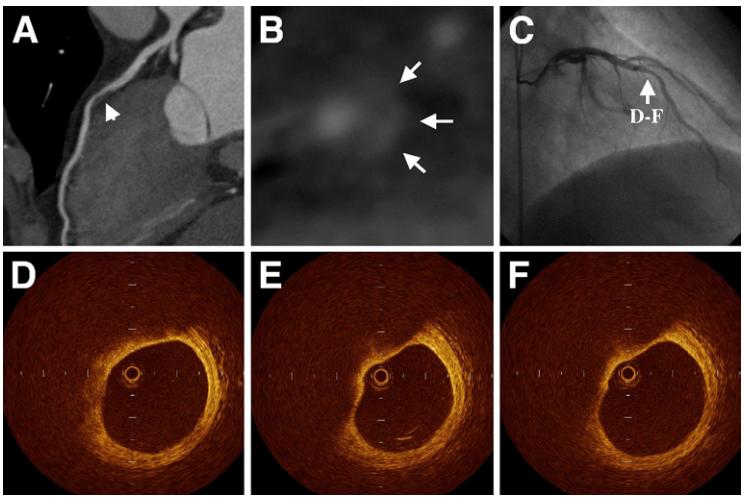

Figure 4. Another Case With Ring-Like Enhancement

(A and B) Another representative image of the ring-like enhancement **(white arrows)** assessed by multidetector computed tomography is shown. This ring-like enhancement is located in the midportion of left anterior descending artery. **(C)** Invasive angiography revealed moderate stenosis in the midportion of left anterior descending artery. **(D** [proximal] to **F** [distal]) Optical coherence tomography clearly identified an eccentric plaque covered with thin fibrous cap at the corresponding site.

patients with TCFA. In the TCFA group, however, there were no differences in mean heart rate between patients showing ring-like enhancement and those without (66 ± 9 beats/min and 64 ± 5 beats/min, p = 0.49).

DISCUSSION

MDCT for TCFA. We demonstrated the differences of the morphologies present in TCFA and non-TCFA as detected by 64-slice MDCT in this study. Pathological studies have suggested that TCFA is a precursor lesion for ACS (24). Therefore, in order to prevent ACS events, noninvasive assessment of TCFA has been investigated for a long time. MDCT has the potential for noninvasive assessment of coronary plaques. Therefore, many investigators have studied the characteristics of culprit plaques in ACS by MDCT (15). Hoffmann et al. (16) have reported that the culprit plaques in ACS showed positive remodeling and noncalcified plaque. Motoyama et al. (15) have concluded that the CT characteristics of plaques associated with ACS include positive vascular remodeling, low plaque attenuation value, and spotty calcification. However, these previous studies used clinical presentations to differentiate between plaque characteristics. Therefore, it would not be certain that a culprit lesion of ACS is derived from a TCFA.

In this study, we applied OCT, which can identify thin fibrous caps and lipid for the detection of TCFA. We revealed that plaque with vascular remodeling and low CT attenuation values are the MDCT morphological features of TCFA, and these results are very similar to previous MDCT studies (15). Although the sensitivity of the RI or the CT attenuation value was higher than that of the ring-like enhancement, our stepwise regression analysis clearly showed that ring-like enhancement, not remodeling was the most important morphological correlate of MDCT for TCFA. Although the ring-like enhancement has a very high specific-

Table 1. Patient Characteristics

	TCFA Group (n = 25)	Non-TCFA Group (n = 80)	p Value
Age (yrs)	66 ± 9	67 ± 11	0.68
Men	21 (84%)	64 (80%)	0.88
Body weight (kg)	65 ± 11	63 ± 9	0.36
Acute coronary syndrome	13 (52%)	18 (23%)	0.01
Hypertension	13 (52%)	41 (51%)	1.00
Diabetes mellitus	6 (24%)	26 (33%)	0.58
Hypercholesterolemia (>220 mg/dl)	11 (44%)	39 (49%)	0.85
Smoking	8 (32%)	31 (39%)	0.71
Family history of ischemic heart disease	3 (12%)	10 (13%)	1.00
Heart rate at CT scanning	62 ± 10	64 ± 12	0.45
High-sensitive CRP (mg/dl)	0.32 ± 0.32	0.17 ± 0.16	<0.001

Data are presented as mean ± SD or n (%).
CRP = C-reactive protein; CT = computed tomography; TCFA = thin-cap fibroatheroma.

ity of 97% for detecting TCFA, it only showed a sensitivity of 44%. It is most likely that the ring-like enhancement would become a sensitive marker of TCFA with increasing resolution of future scanner generations.

Raffel et al. (25) reported a close association between positive coronary artery remodeling and TCFA in a recent IVUS and OCT study. From these results, the plaque contents, especially lipid contents, might be considered to grow both outward from and inward toward the lumen. Finally, a boundary-growing plaque may fall into catastrophic ACS events. Our recent IVUS and MDCT study had revealed that plaque area of ruptured plaque was larger than that of nonruptured plaque (18). However, we did not find a difference in plaque area between TCFA and non-TCFA in this study, and one-half of our TCFA group showed a stable clinical presentation. While TCFA is recognized as one of the precursor lesions for ACS, there are few data regarding the timeline from TCFA to rupture; some TCFAs may require longer time for more plaque growth and rupture. Further study is needed to clarify this issue.

Ring-like enhancement and TCFA. Our previous IVUS and MDCT study had revealed that a ring-like enhancement is associated with ruptured plaques, and suggested that a ring-like enhancement would reflect a precursor lesion (18). The available data from this study verified that a ring-like enhancement observed by MDCT was one important sign of TCFA. We have considered 3 possible explanations for this imaging phenomenon.

First, the ring-like enhancement is very similar in shape to the mantle sign that appears in inflammatory aortic abdominal aneurysms imaged by enhanced CT (26,27). The peripheral enhancement of the aortic wall is thought to reflect the neovascularization influenced by active inflammation. Similarly, coronary arteries contain a network of vasa vasorum neovascularization in the adventitia. This vasa vasorum of the coronary artery was well visualized by the micro-CT technique (28). The micro-CT studies have suggested that proliferation of vasa vasorum is part of the response to the injury phenomenon in the process of plaque formation. Inflammation and pathological neovascularization are thought to precipitate plaque rupture and cardiovascular events (29). It is also reported that neovessel formation strongly correlates with macrophage infiltration in atherosclerotic plaque, suggesting vasa vasorum density as a surrogate marker of plaque vulnerability (30). We speculate that the ring-like enhancement reflects this highly active vasa vasorum neovascularization in vulnerable plaque.

An alternative explanation is that coronary plaque with lipid-rich content shows a lower CT attenuation value compared with the native vessel wall or fibrous plaque (16). In cases with plaque that contains small amounts of lipid content, the CT attenuation value of the coronary plaque may present as low, but it would be difficult for MDCT to separate the lipid contents from fibrous contents

Table 2. Invasive Angiographic Findings

	TCFA Group (n = 25)	Non-TCFA Group (n = 80)	p Value
Culprit site			
Left descending artery	10 (40%)	42 (53%)	0.39
Proximal	6 (24%)	21 (26%)	1.00
Mid	4 (16%)	20 (25%)	0.51
Distal	0 (0%)	1 (1%)	1.00
Left circumflex artery	3 (12%)	15 (19%)	0.63
Proximal	1 (4%)	4 (5%)	1.00
Mid	1 (4%)	5 (6%)	1.00
Distal	1 (4%)	6 (8%)	0.87
Right coronary artery	12 (48%)	23 (29%)	0.12
Proximal	5 (20%)	8 (10%)	0.33
Mid	4 (16%)	9 (11%)	0.78
Distal	3 (12%)	6 (8%)	0.77
Single-vessel disease	13 (52%)	38 (48%)	0.87
QCA data			
Minimal lumen diameter (mm)	0.8 ± 0.6	0.8 ± 0.6	1.00
Reference diameter (mm)	3.2 ± 0.7	3.0 ± 0.6	0.18
% Diameter stenosis	76.6 ± 17.4	71.9 ± 20.9	0.31

Data are presented as n (%) or mean ± SD.
QCA = quantitative coronary angiography; TCFA = thin-cap fibroatheroma.

Table 3. Comparison Between OCT and MDCT

	TCFA Group (n = 25)	Non-TCFA Group (n = 80)	p Value
Ring-like enhancement	11 (44%)	3 (4%)	<0.0001
Calcium deposition			
Long (>3 mm)	2 (8%)	20 (25%)	0.12
Short (≤3 mm)	9 (36%)	23 (29%)	0.66
None	14 (56%)	37 (46%)	0.53
Outer vessel area (mm^3)	21.9 ± 6.5	19.5 ± 5.3	0.06
Luminal area (mm^3)	6.1 ± 3.7	6.4 ± 4.3	0.75
% Plaque area	70.2 ± 20.3	66.6 ± 21.3	0.46
Positive remodeling	19 (76%)	25 (31%)	<0.001
Remodeling index	1.14 ± 0.15	1.02 ± 0.10	<0.0001
CT attenuation value (HU)	35.1 ± 32.3	62.0 ± 33.6	<0.001

Data are presented as n (%) or mean ± SD.
MDCT = multidetector computed tomography; OCT = optical coherence tomography; other abbreviations as in Table 1.

Table 4. Results of Stepwise Regression Analysis

	Beta-Coefficients	p Value
Ring-like enhancement	0.482	<0.01
High-sensitive CRP	0.249	<0.01
Acute coronary syndrome	0.235	<0.01
CT attenuation value		0.07
Remodeling index		0.18
Age		0.56
Sex		0.68

Abbreviations as in Table 1.

or native vessel wall because of its limited spatial resolution. Conversely, in cases with plaque showing large positive remodeling and large lipid contents, both morphological features of TCFA, MDCT could separate lipid contents from other structures except the thin fibrous cap. These figures would be represented in the ring-like enhancement.

Finally, the ring-like enhancement also resembles the image of thrombosis (31). Although the frequency of thrombus was not significantly different between the 2 groups, there is a possibility that the ring-like enhancement could be related to the presence of thrombus.

Clinical implication. Although OCT can visualize TCFA in vivo, being an invasive method limits the clinical application of OCT to search for TCFA. As such, identification of TCFA noninvasively by MDCT would allow identification of the high-risk patients and would contribute to the management and prevention of ACS events.

Study limitations. A number of limitations can be said to be associated with the present study. We excluded many patients with chronic renal failure who were on dialysis because of the predilection to severe calcification. Also, cardiogenic shock and heart failure patients were excluded due to additional OCT analysis. Therefore, the study population was relatively small, and our results may not be applicable to all patients with coronary artery disease. Also, the surrounding contrast enhancement might influence the density measurements within plaque.

CONCLUSIONS

MDCT verified ring-like enhancement may allow identification of TCFA and may provide the noninvasive assessment of vulnerable plaque.

Reprint requests and correspondence: Dr. Atsushi Tanaka, Department of Cardiovascular Medicine, Wakayama Medical University, 811-1, Kimiidera, Wakayama 641-8509, Japan. *E-mail: a-tanaka@wakayama-med.ac.jp.*

REFERENCES

1. Falk E. Plaque rupture with severe pre-existing stenosis precipitating coronary thrombosis: characteristics of coronary atherosclerotic plaques underlying fatal occlusive thrombi. Br Heart J 1983;50:127–34.
2. Virmani R, Kolodgie FD, Burke AP, et al. Lessons from sudden coronary death: a comprehensive morphological classification scheme for atherosclerotic lesions. Arterioscler Thromb Vasc Biol 2000;20:1262–75.
3. Fustre V, Stein B, Ambrose JA, et al. Atherosclerotic plaque rupture and thrombosis. Evolving concepts. Circulation 1990;82:II47–59.
4. Jang IK, Bouma BE, Kang DH, et al. Visualization of coronary atherosclerotic plaques in patients using optical coherence tomography: comparison with intravascular ultrasound. J Am Coll Cardiol 2002;39:604–9.
5. Brezinski ME, Tearney GJ, Bouma BE, et al. Optical coherence tomography for optical biopsy. Properties and demonstration of vascular pathology. Circulation 1996;93:1206–13.
6. Kume T, Akasaka T, Kawamoto T, et al. Visualization of neointima formation by optical coherence tomography. Int Heart J 2005;46:1133–6.
7. Kume T, Akasaka T, Kawamoto T, et al. Assessment of coronary intima media thickness by optical coherence tomography: comparison with intravascular ultrasound. Circ J 2005;69:903–7.
8. Kume T, Akasaka T, Kawamoto T, et al. Assessment of coronary arterial plaque by optical coherence tomography. Am J Cardiol 2006;97:1172–5.
9. Jang IK, Tearney GJ, MacNeill B, et al. In vivo characterization of coronary atherosclerotic plaque by use of optical coherence tomography. Circulation 2005;111:1551–5.
10. Kume T, Akasaka T, Kawamoto T, et al. Measurement of the thickness of the fibrous cap by optical coherence tomography. Am Heart J 2006;152:755.e1–4.
11. Hoffmann U, Nagurney JT, Moselewski F, et al. Coronary multidetector computed tomography in the assessment of patients with acute chest pain. Circulation 2006;114:2251–60.
12. Rubinshtein R, Halon DA, Gaspar T, et al. Usefulness of 64-slice cardiac computed tomographic angiography for diagnosing acute coronary syndromes and predicting clinical outcome in emergency department patients with chest pain of uncertain origin. Circulation 2007;115:1762–8.
13. Achenbach S. Computed tomography coronary angiography. J Am Coll Cardiol 2006;48:1919–28.
14. Schroeder S, Kopp AF, Baumbach A, et al. Noninvasive detection and evaluation of atherosclerotic coronary plaques with multislice computed tomography. J Am Coll Cardiol 2001;37:1430–5.
15. Motoyama S, Kondo T, Sarai M, et al. Multislice computed tomographic characteristics of coronary lesions in acute coronary syndromes. J Am Coll Cardiol 2007;50:319–26.
16. Hoffmann U, Moselewski F, Nieman K, et al. Noninvasive assessment of plaque morphology and composition in culprit and stable lesions in acute coronary syndrome and stable lesions in stable angina by multidetector computed tomography. J Am Coll Cardiol 2006;47:1655–62.

17. Nakazawa G, Tanabe K, Onuma Y, et al. Efficacy of culprit plaque assessment by 64-slice multidetector computed tomography to predict transient no-reflow phenomenon during percutaneous coronary intervention. Am Heart J 2008;155:1150–7.
18. Tanaka A, Shimada K, Yoshida K, et al. Non-invasive assessment of plaque rupture by 64-slice multidetector computed tomography. Circ J 2008; 72:1276–81.
19. Hoffmann U, Nagurney JT, Moselewski F, et al. Coronary multidetector computed tomography in the assessment of patients with acute chest pain. Circulation 2006;114:2251–60.
20. Kataiwa H, Tanaka A, Kitabata H, et al. Safety and usefulness of non-occlusion image acquisition technique for optical coherence tomography. Circ J 2008;72:1536–7.
21. Yabushita H, Bouma BE, Houser SL, et al. Characterization of human atherosclerosis by optical coherence tomography. Circulation 2002;106: 1640–5.
22. Kubo T, Imanishi T, Takarada S, et al. Assessment of culprit lesion morphology in acute myocardial infarction ability of optical coherence tomography compared with intravascular ultrasound and coronary angiography. J Am Coll Cardiol 2007;50:933–9.
23. Tanaka A, Imanishi T, Kitabata H, et al. Morphology of exertion-triggered plaque rupture in patients with acute coronary syndrome: an optical coherence tomography study. Circulation 2008;118:2368–73.
24. Falk E, Shah PK, Fuster V. Coronary plaque disruption. Circulation 1995; 92:657–71.
25. Raffel OC, Merchant FM, Tearney GJ, et al. In vivo association between positive coronary artery remodeling and coronary plaque characteristics assessed by intravascular optical coherence tomography. Eur Heart J 2008; 29:1721–8.
26. Rasmussen TE, Hallett JW Jr. Inflammatory aortic aneurysms. A clinical review with new perspectives in pathogenesis. Ann Surg 1997;225: 155–64.
27. Gomes MN, Choyke PL. Infected aortic aneurysms: CT diagnosis. J Cardiovasc Surg (Torino) 1992;33: 684–9.
28. Kwon HM, Sangiorgi G, Ritman EL, et al. Enhanced coronary vasa vasorum neovascularization in experimental hypercholesterolemia. J Clin Invest 1998;101:1551–6.
29. Fleiner M, Kummer M, Mirlacher M, et al. Arterial neovascularization and inflammation in vulnerable patients: early and late signs of symptomatic atherosclerosis. Circulation 2004;110: 2843–50.
30. Maehara A, Mintz GS, Bui AB, et al. Morphologic and angiographic features of coronary plaque rupture detected by intravascular ultrasound. J Am Coll Cardiol 2002;40:904–10.
31. Zerhouni EA, Barth KH, Siegelman SS. Demonstration of venous thrombosis by computed tomography. AJR Am J Roentgenol 1980;134:753–8.

Key Words: imaging ■ plaque ■ computed tomography ■ tomography ■ optical coherence.